

Electronic Supplementary Information

Patchy rough colloids as Pickering stabilizers

Hannah M. H. Weijgertze,[†] Willem K. Kegels^{†}, Michele Zanini^{†*}*

† Van 't Hoff Laboratory for Physical and Colloid Chemistry, Debye Institute for
Nanomaterials Science, Utrecht University, Utrecht (The Netherlands)

KEYWORDS: Patchy colloids. Rough colloids, Pickering emulsions, Emulsion phase inversion.

S1. Homogeneous nucleation of TPM

To verify that TPM particle size increases with increasing volume fraction of TPM in the reaction mixture at constant pH, TPM particles were produced via homonucleation in the following manner: 25, 30, 35, 42 or 50 μL TPM was added to 16 mL water in a 50 mL polypropylene centrifuge tube brought at pH 10.4 by addition of NH_3 . After agitation on a tumbling table at 150 rpm for 90 min, 8 mg AIBN was added. The tube was brought under N_2 and tumbled in an oil bath (80°C) for 2 hours. After washing the resulting particles by centrifugation, SEM images (Phenom ProX) were taken from which the particle sizes were determined. Figure S1 shows the observed nearly linear increase of TPM particle size with volume fraction of TPM in the reaction mixture. This principle was exploited for the synthesis of the patchy rough particles.

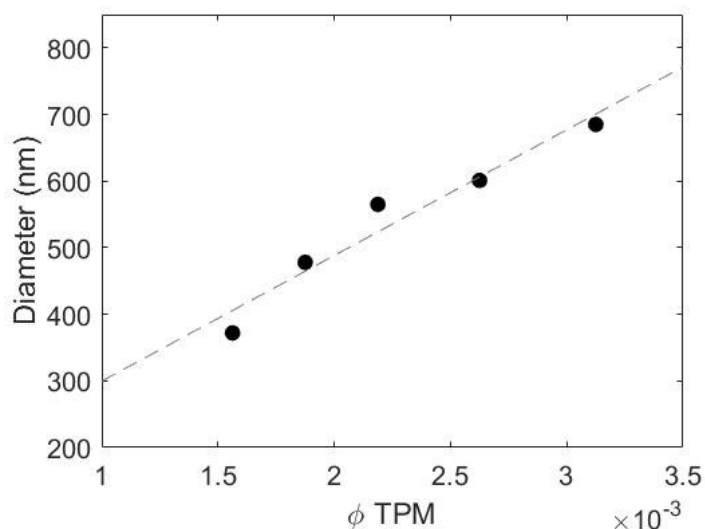


Figure S1. Homogeneous nucleation of TPM. The graph shows the increase in TPM particle size with increasing volume fraction (Φ) TPM in the reaction mixture.

TPM particles for GTT and emulsification

TPM particles of 797 ± 109 nm in diameter were produced by homogeneous nucleation of TPM in a scaled-up synthesis yielding over half a gram of particles. For this, 2.7 mL TPM was added to 800 mL water and 200 μL NH_3 in a Teflon bottle. After agitation of the mixture for 2 hours on a tumbling table (to accommodate the formation of TPM droplets) the mixture was transferred to a 2L round-bottomed flask. To this, 260 mg of the polymerization initiator AIBN was added and the flask was deoxygenated with N_2 . The polymerization of the TPM spheres was carried out under

magnetic stirring in an oil bath (80°C) for 2 hours. The resulting particles were washed three times by centrifugation at $3270 \times g$. The particle size was determined from SEM (Phenom ProX), see Figure S2. These particles were used for GTT contact angle measurements and for producing reference emulsions.

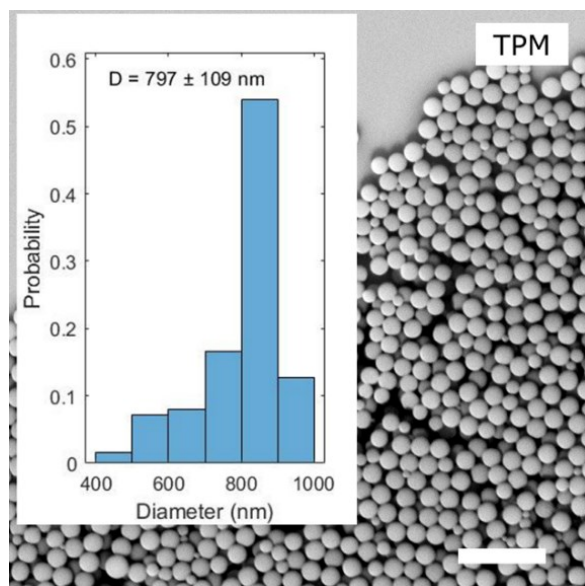


Figure S2. Size distribution of the TPM particles determined from the SEM image. Scale bar: 4 μm .

S2. TGA calculation

For the estimation of the mass% TPM in the patchy rough particles, first the residual masses upon calcination of pure PS and TPM were determined. With these quantities and the dry and residual masses of the patchy rough particles, the composition of these particles in mass% TPM was calculated.

Calculated quantities from reference measurements:

- Pure PS residual mass fraction (PSrMf)
- Pure TPM residual mass fraction (TPMrMf)

Weighed quantities from patchy rough particle measurements:

- Particle mass after drying (drym)
- Residual mass after calcination (resm)

Since the patchy rough particles are composed of both PS and TPM, the drym consists of the dried TPM mass (dTPMm) and dried PS mass (dPSm), and the resm consists of the residual TPM mass (rTPMm) and residual PS mass (rPSm). In equations:

$$dPSm + dTPMm = drym$$

$$rPSm + rTPMm = resm$$

These equations are coupled by:

$$PSrMf * dPSm = rPSm$$

$$TPMrMf * dTPMm = rTPMm$$

Combining these equations gives the following system of equations, solvable for dTPMm:

$$PSrMf * (drym - dTPMm) = resm - rTPMm$$

$$rTPMm = TPMrMf * dTPMm$$

The mass% TPM in the patchy rough particles is then $dTPMm/drym*100\%$.

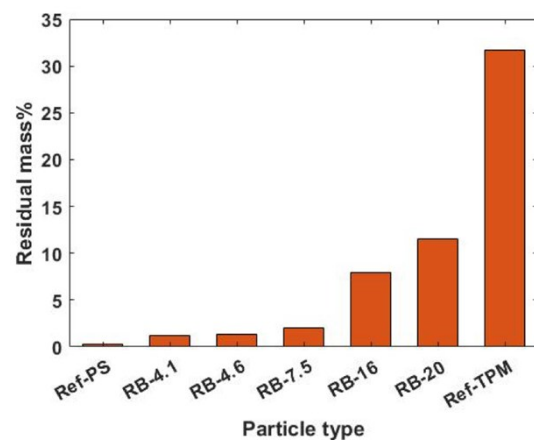


Figure S3. Residual particle masses after degradation upon calcination.

S3. SEM images for surface patchiness

Figure S4 and Figure S5 show representative SEM images from which the surface patchiness of the patchy rough particles was estimated. Each left image shows the asperity size measurement and each right image the estimation of the number of asperities on a sphere.

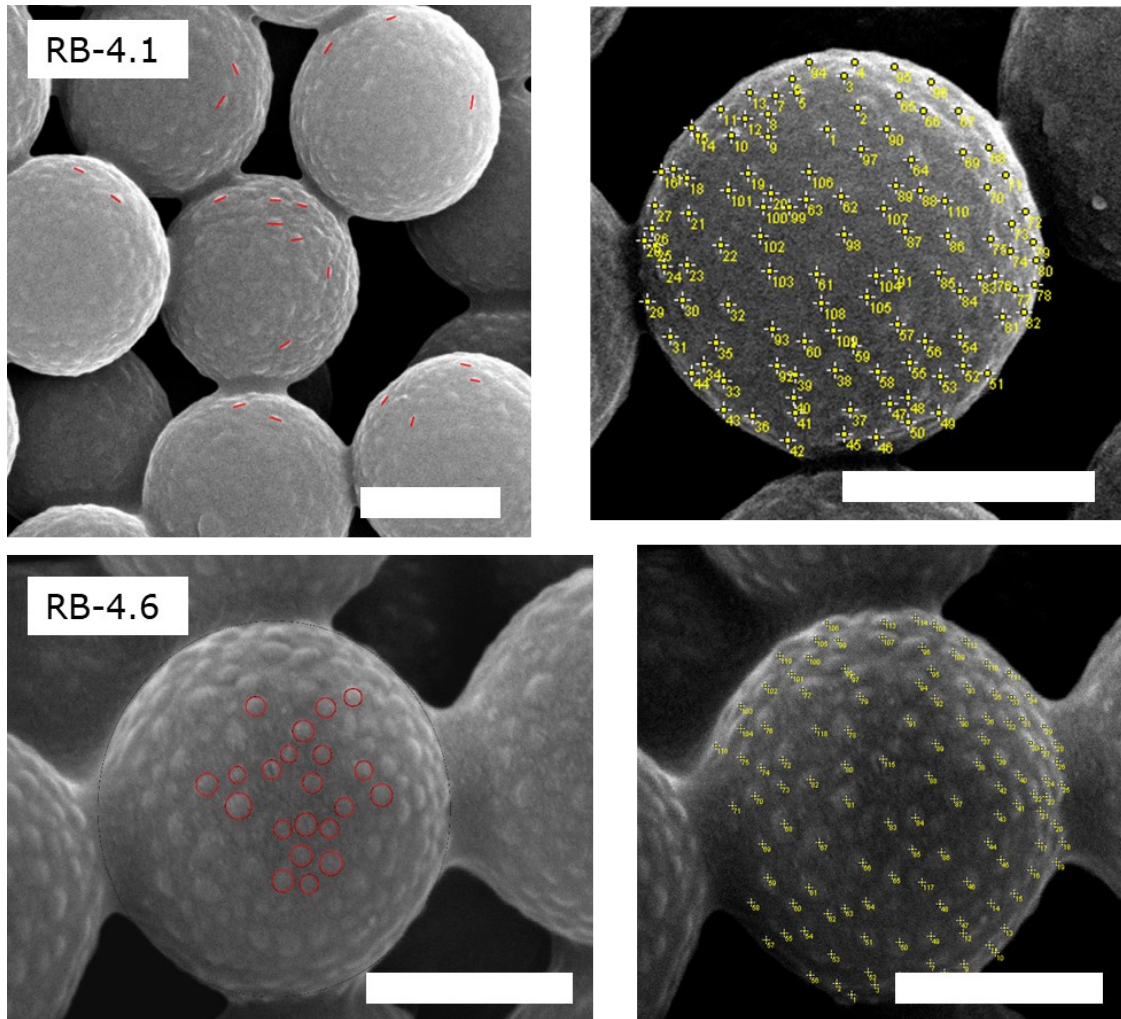


Figure S4. Representative SEM images for surface patchiness estimation of RB-4.1 and RB-4.6. Scalebars: 500 nm.

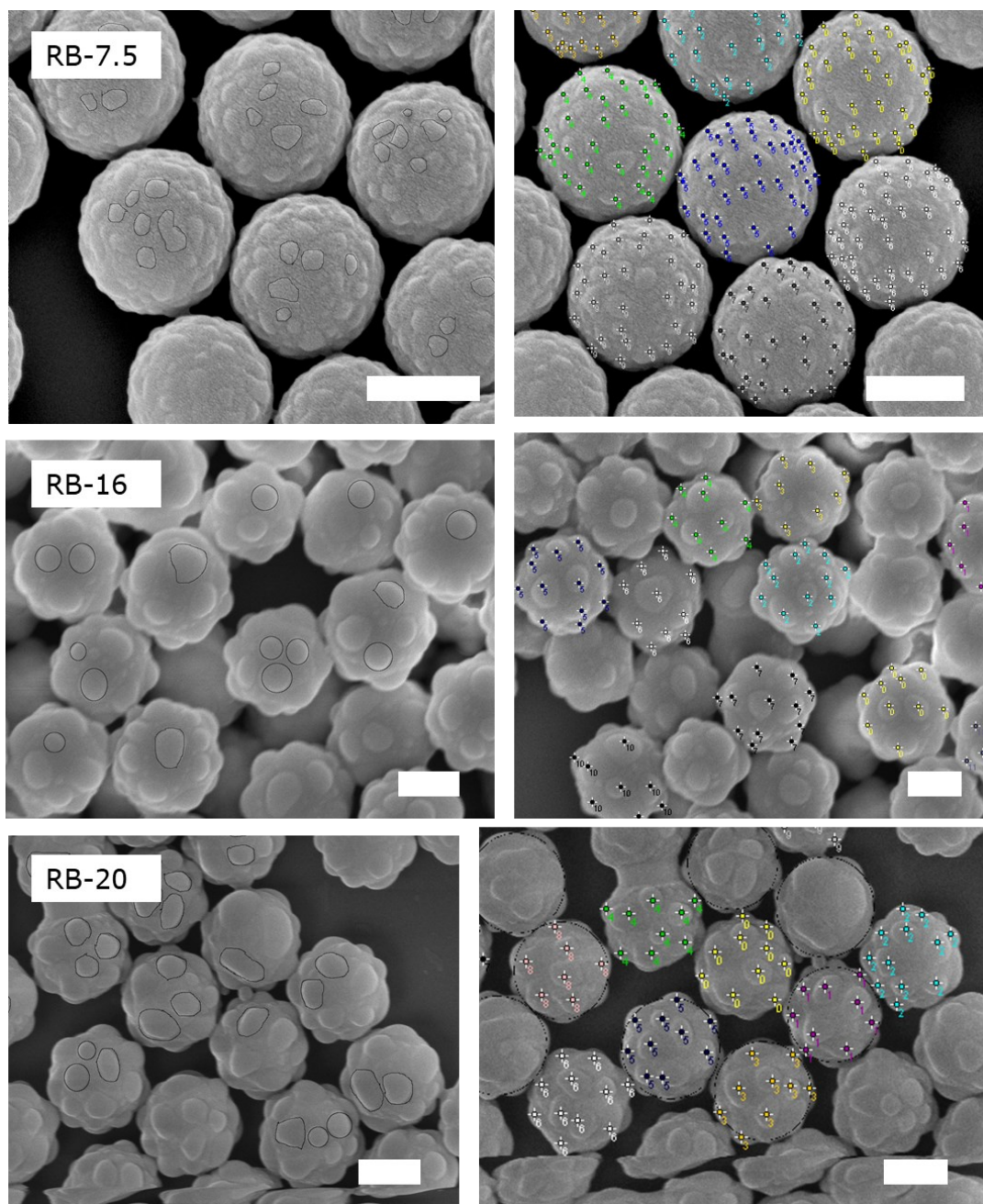


Figure S5. Representative SEM images for surface patchiness estimation of RB-7.5, RB-16 and RB-20. Scalebars: 500 nm.

S4. GTT contact angle calculation

This section contains details on the contact angle calculations from SEM images of interface replicas produced by GTT. Figure S6 shows representative images used for the contact angle calculations. At least 70 particles of each particle type were involved in the calculations.

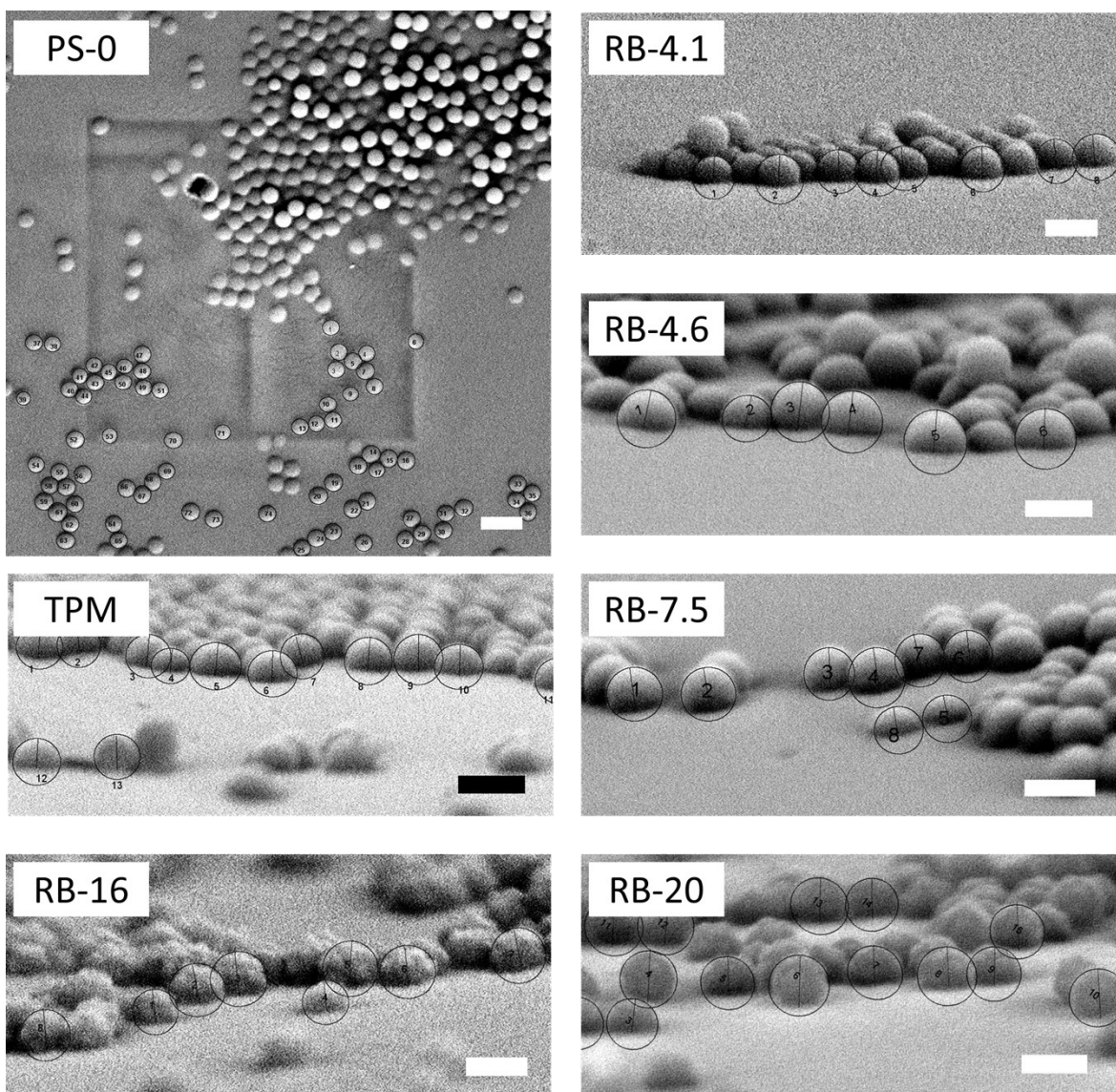


Figure S6. Representative SEM images of interface replicas with PS, TPM and the raspberry-like particles. Scalebars: PS-0: 2 μm , other scalebars: 1 μm .

Contact angles of PS-0 were determined from top views of the interface. A top view image looks through the water phase on the oil phase (which is replaced by UV glue). In this configuration, the

largest portion of a hydrophobic particle is immersed in the UV glue. Then, by comparing the particle radius at the interface with the actual particle radius independently obtained, the contact angle of the particle at the interface can be extracted according to the following relation (which is visualized in Figure S7):

$$\theta = \theta_w = \sin^{-1}\left(\frac{S}{R}\right) \#(3)$$

where S is the radius at the interface determined from the SEM image of the replica and R is the average particle radius as given in Figure S9.

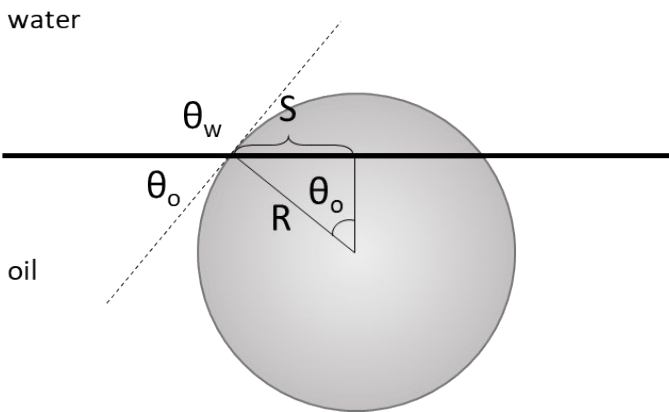


Figure S7. The contact angle of a hydrophobic particle on the interface can be calculated from a top view SEM image by measuring the radius on the interface S and using the illustrated geometry.

Contact angles of the hydrophilic particles were determined from a cross-section of the interface. By measuring the height of the spherical cap H and the particle radius r on the SEM images of the interface replicas (see Figure S8), the contact angle can be found using the following relation:

$$\theta = \cos^{-1}\left(\frac{|H - r|}{r}\right) \#(4)$$

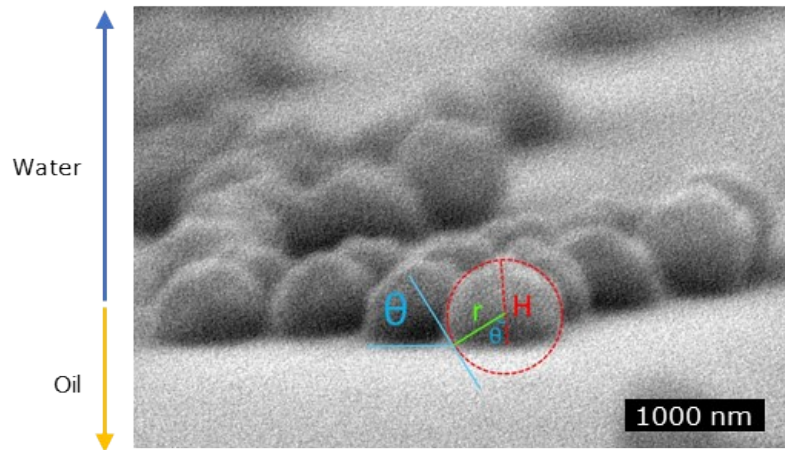


Figure S8. Cross-section of an interface replica. The contact angle can be calculated from the measured cap height H and particle radius r .

S5. Reproducibility of PS core synthesis

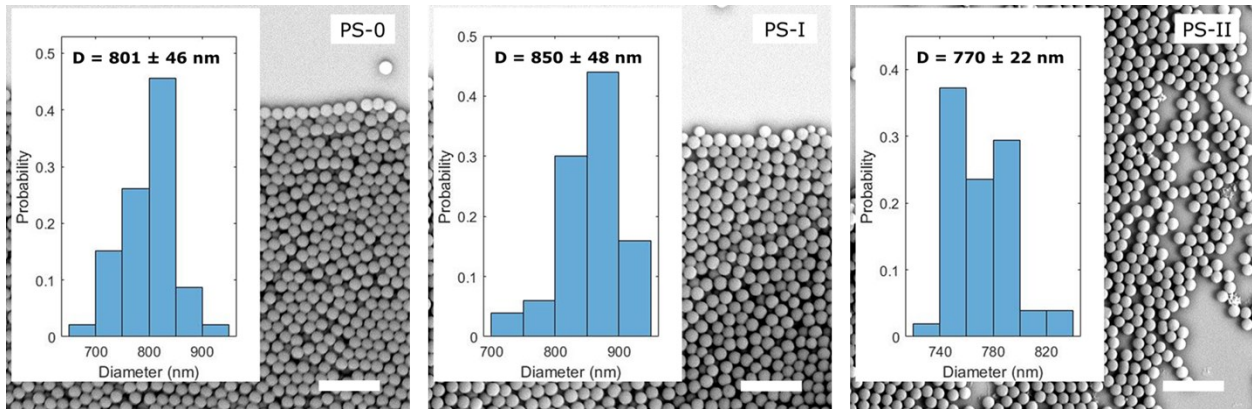


Figure S9. SEM images of polystyrene (PS) particles and size distributions determined from the images. Scalebars: 4 μ m.

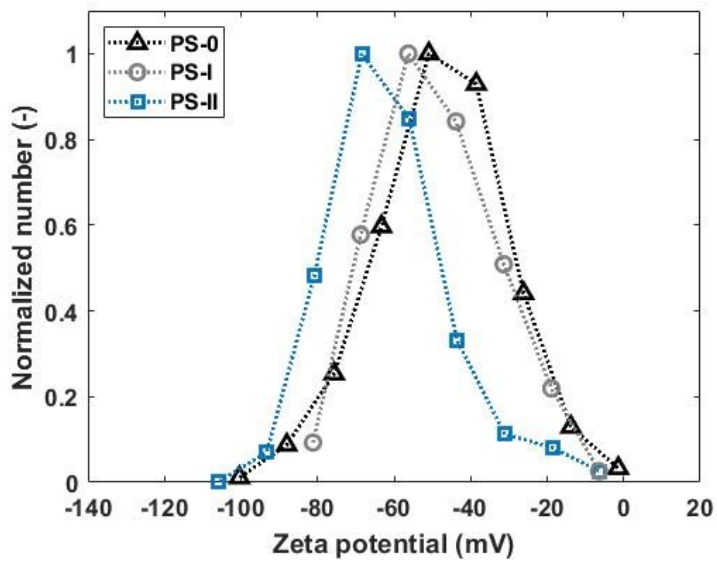


Figure S10. Zeta potential distributions of the PS cores used for the patchy rough colloid synthesis.

S6. Reaction window PS/TPM colloid fabrication

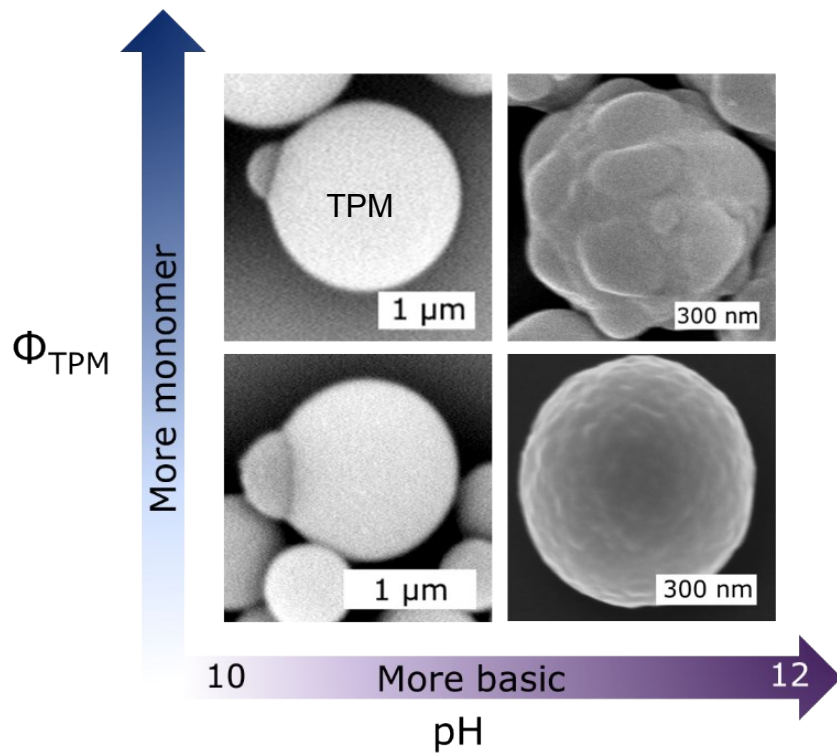


Figure S11. Dependence of the surface morphology of PS/TPM colloids on the volume fraction (ϕ) TPM and pH.

S7. Overview of produced patchy rough particles

Table S1. Fabricated patchy rough particles in this work. pH = 11.5.

Patchy rough particle	PS core	Vol% TPM
RB-4.1	PS-0	0.17
RB-4.6	PS-I	0.20
RB-7.5	PS-II	0.22
RB-16	PS-I	0.25
RB-20	PS-0	0.32

S8. Effect of BODIPY on interfacial tensions and emulsification

Interfacial tensions of water and n-decane were measured at different concentration of BODIPY 493/503 to evaluate the effect of the BODIPY addition. At the same conditions, emulsions of the two phases in the absence of particles were prepared. The reason for measuring the interfacial tensions is that BODIPY can act as a surfactant, and the creation of surfactant emulsions relies on the lowering of the interfacial tension upon adsorption of surface active molecules.¹ Figure S12 shows the slight decrease in interfacial tension with increasing concentration of BODIPY in n-decane.

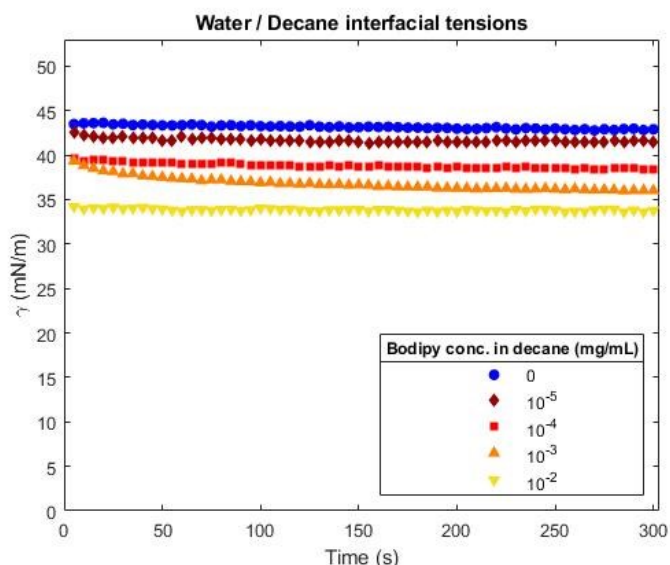


Figure S12. Water / n-decane interfacial tensions (γ) at different concentrations of BODIPY in n-decane. Interfacial tensions were measured with a dataphysics OCA15plus Contact angle system by creating a water pendant drop² from a syringe with a dataphysics SNP-D 165/135 needle in a BODIPY/n-decane phase in an optical cuvette (Hellma 100-05).

Although the lowering of the water-decane interfacial tensions shows that BODIPY adsorbs on the interface, the used BODIPY concentrations do not produce significant emulsions (only some tiny white flakes are observed after 'emulsification', see Figure S13). Therefore, it is not expected that the addition of BODIPY to the emulsion formulations containing particles will affect the emulsification. Still, to avoid any unexpected interference with the emulsification, the emulsions were prepared with the lowest possible concentration of BODIPY.

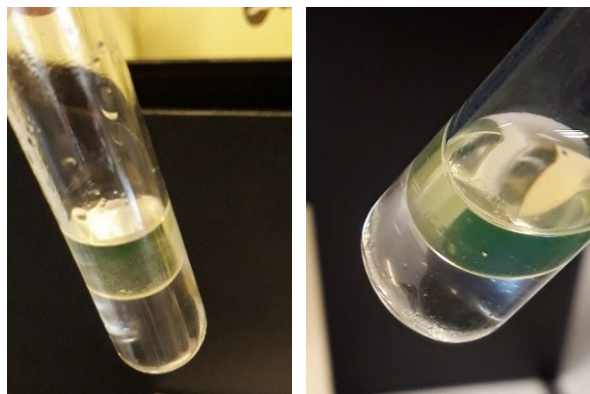


Figure S13. 'Emulsification' of 10⁻³ (left) and 10⁻² (right) mg/mL BODIPY in n-decane with water.

S9. Emulsification challenges using RB-20

It was noted that RB-20 particles usually do not form emulsions with droplets finely dispersed in the continuous phase, or even only form clumps of emulsion that stick to the tube walls and are easily destroyed by gentle handshaking. To a lesser extent, such limited emulsification was also sometimes observed for RB-16. Figure S14 shows typical bright field microscopy images of emulsions with RB-20. The non-continuous structure of the emulsions is also visible in the macroscopic photograph in Figure S14. Clusters of droplets, sometimes encapsulated by a film, cannot be separated without destroying the emulsion. A cause for this might be limited adsorption of the particles on the oil-water interface and extensive particle bridging.

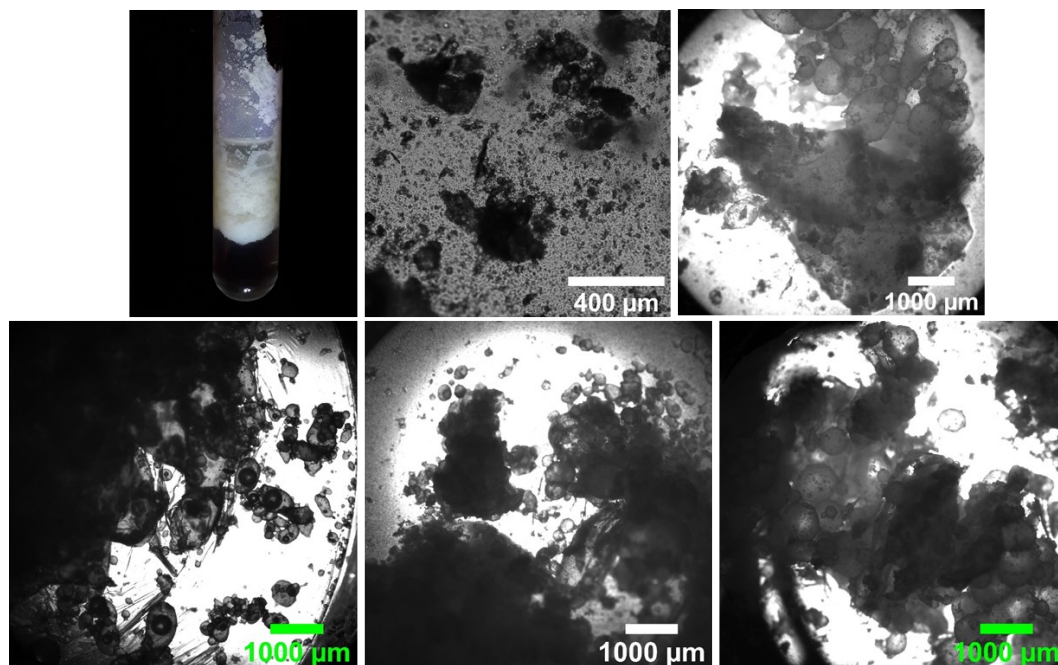


Figure S14. Typical images of emulsions with RB-20 particles. Instead of finely dispersed droplets, clumps of droplets in various morphologies are present.

The adsorption of particles on a droplet might be limited due to a too high surface charge of the particles or due to the presence of many surface active molecules in the particle suspensions. The adsorption of a highly charged particle might be hindered by electric-double layer repulsion between a particle and the oil-water interface, or by the repulsion between a particle in the water and its image charge (of the same sign) in the oil phase.³ The presence of surfactants might impede the particle adsorption as well. To check whether these effects could play a role in the emulsification of the patchy rough particles, zeta potential and interfacial tension measurements were conducted. Figure S15a shows that the roughest particles have the smallest zeta potentials,

thus are least charged. Increased repulsion between the particles and the interface or their image charge is therefore unlikely to be the cause for the scarce emulsification efficiency. Figure S15b does not show any correlation between the suspensions of rough particles and the interfacial tensions of suspension/n-decane interfaces. Therefore, the presence of surface active species hindering the adsorption of the colloids can also be rejected as cause for limited emulsification with RB-20. Consequently, the roughness of the particles could cause the limited emulsification. Reduced Pickering emulsification stability for particles with a too high degree of roughness has been reported,⁴ and was justified by a wetting transition from the Wenzel regime for particles of lower roughness to the Cassie-Baxter regime for particles of higher roughness.

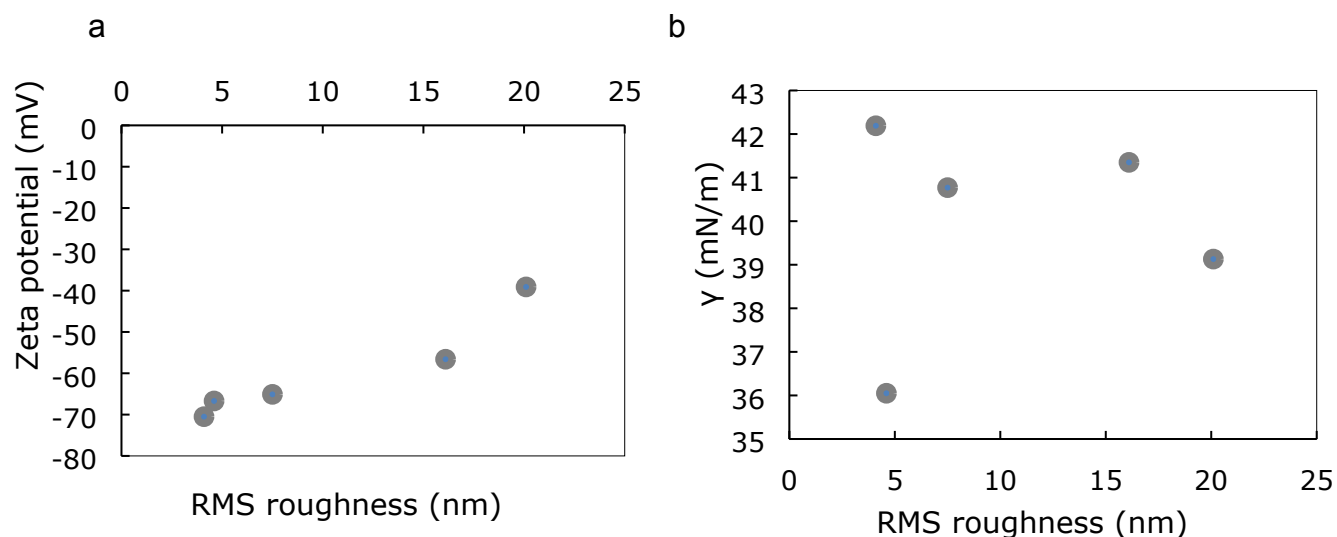


Figure S15. (a) Zeta potentials of patchy rough particles. (b) Interfacial tensions of particle suspensions / n-decane interfaces.

Zeta potential measurements of ~ 0.03 wt% particle suspensions in 10mM KCl were conducted with a Malvern Zetasizer Nano ZS. Interfacial tensions were measured with the same system as described in the caption of Figure S12 of Section S8.

S10. Emulsion phase inversion per particle type

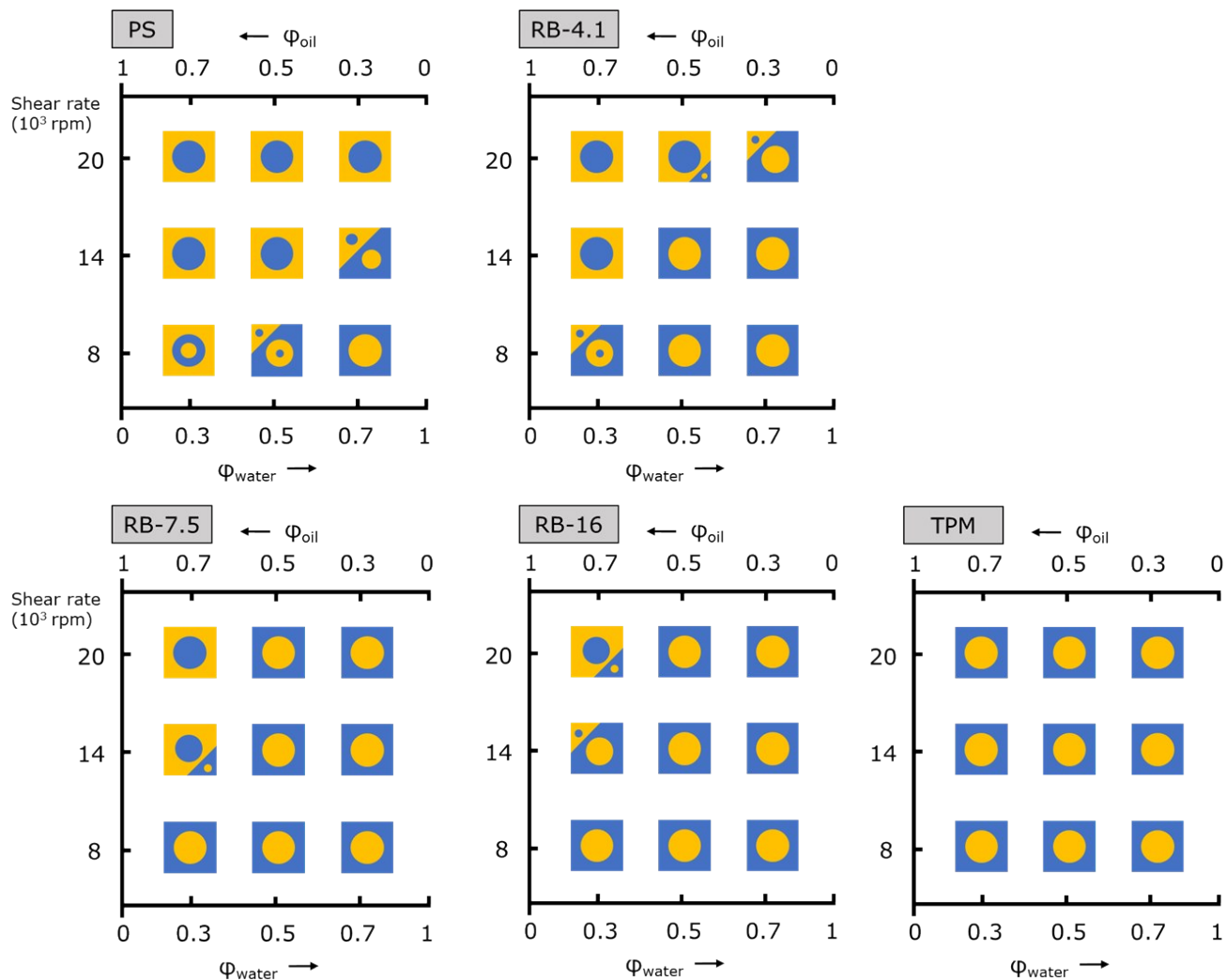


Figure S16. Emulsion phase inversion diagrams per particle type. Increasing the water content (Φ_{water}) in emulsions can result in catastrophic phase inversion. Mechanical phase inversion can occur with increasing emulsification shear rate. No phase inversion is observed for TPM for the probed conditions.

S11. Images of emulsions

In Figure S17 - Figure S21, images of all emulsions supporting the results in Figure S16 are presented. Images are grouped per particle type.

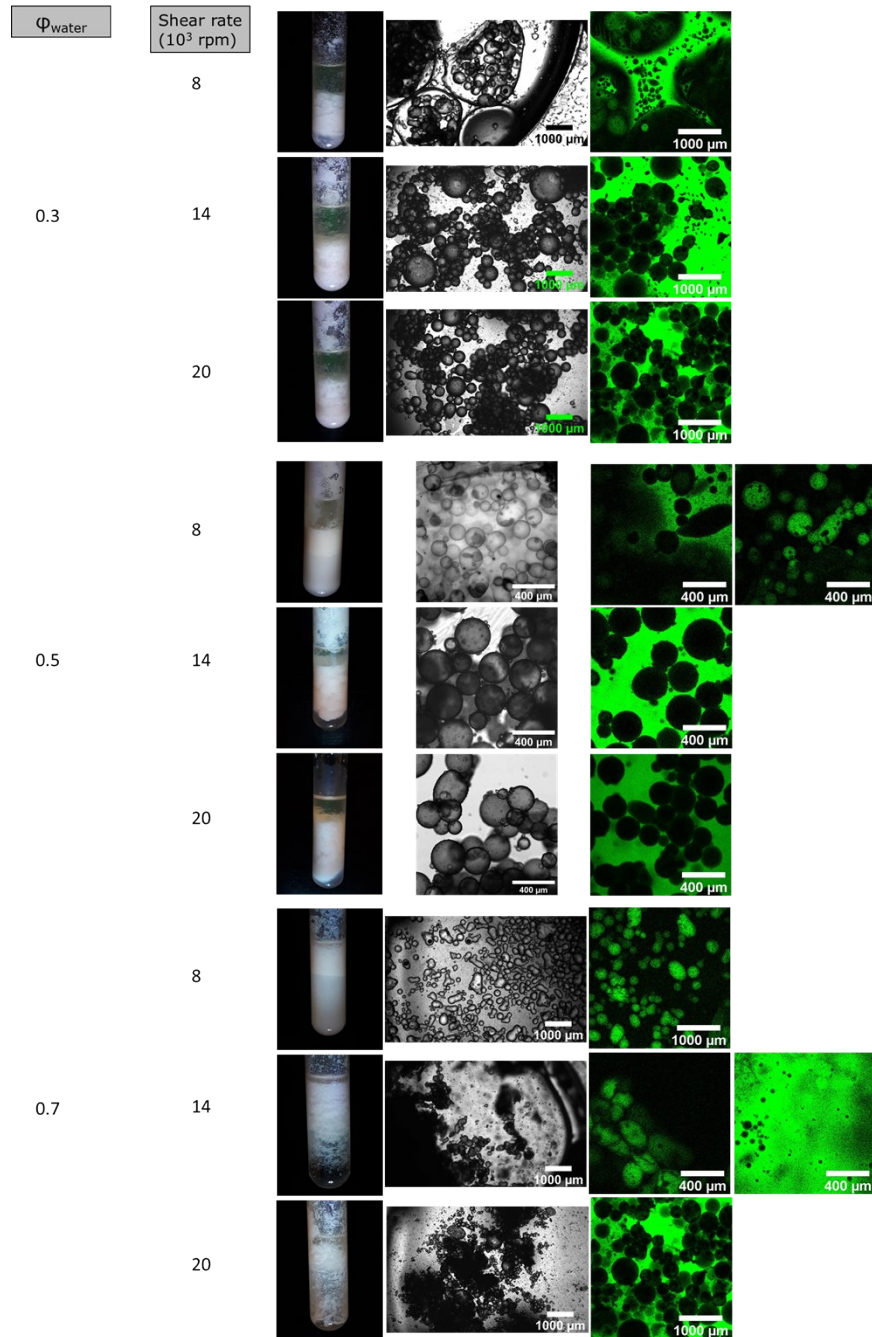


Figure S17. Images of emulsions with PS. From the left to the right column: macroscopic, bright field optical microscopy and confocal fluorescence microscopy images. The confocal fluorescence microscopy images show whether the emulsions are o/w or w/o type by addition of BODIPY 493/503 to the n-decane oil phase.

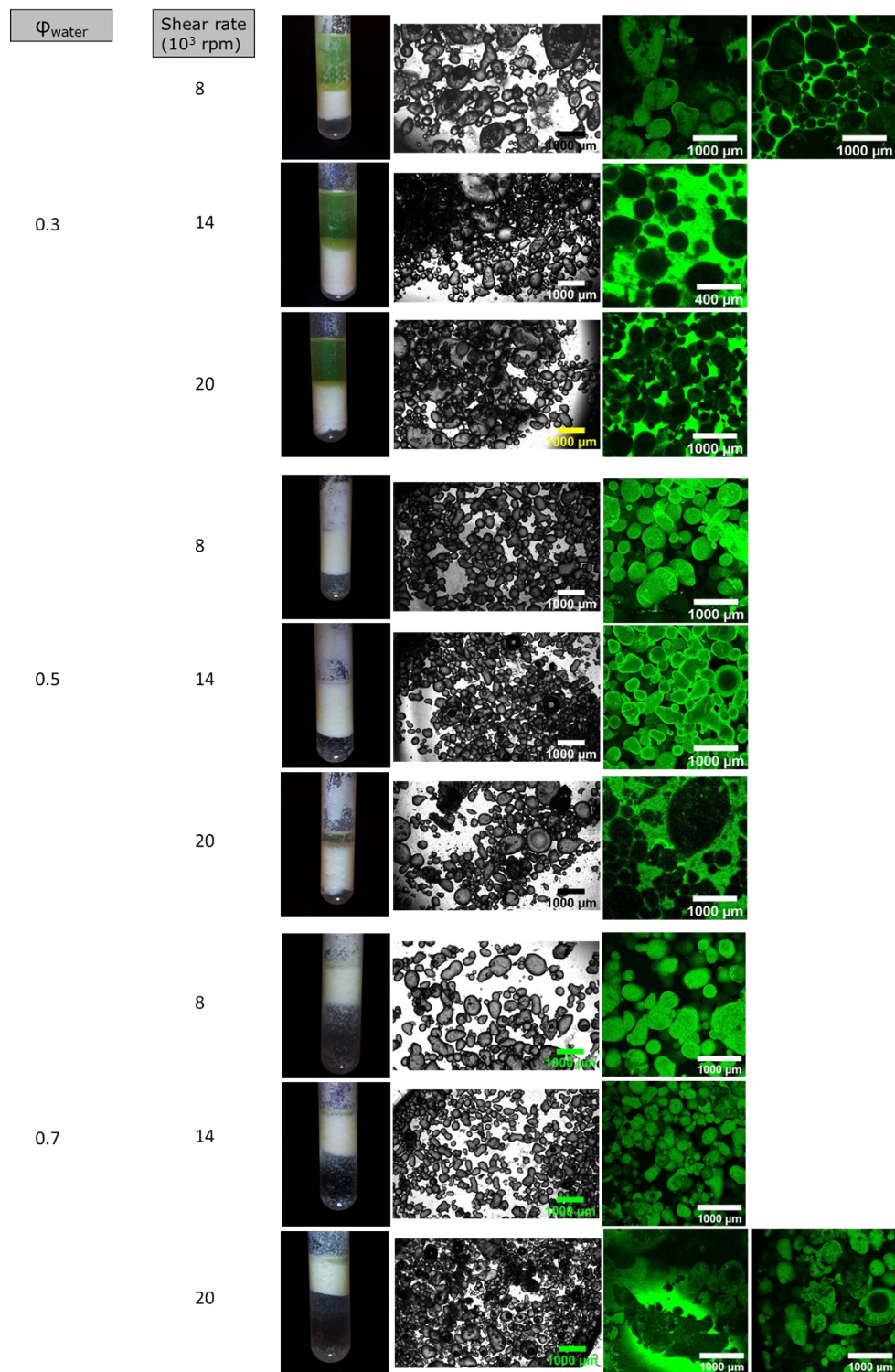


Figure S18. Images of emulsions with RB-4.1. From the left to the right column: macroscopic, bright field optical microscopy and confocal fluorescence microscopy images. The confocal fluorescence microscopy images show whether the emulsions are o/w or w/o type by addition of BODIPY 493/503 to the n-decane oil phase.

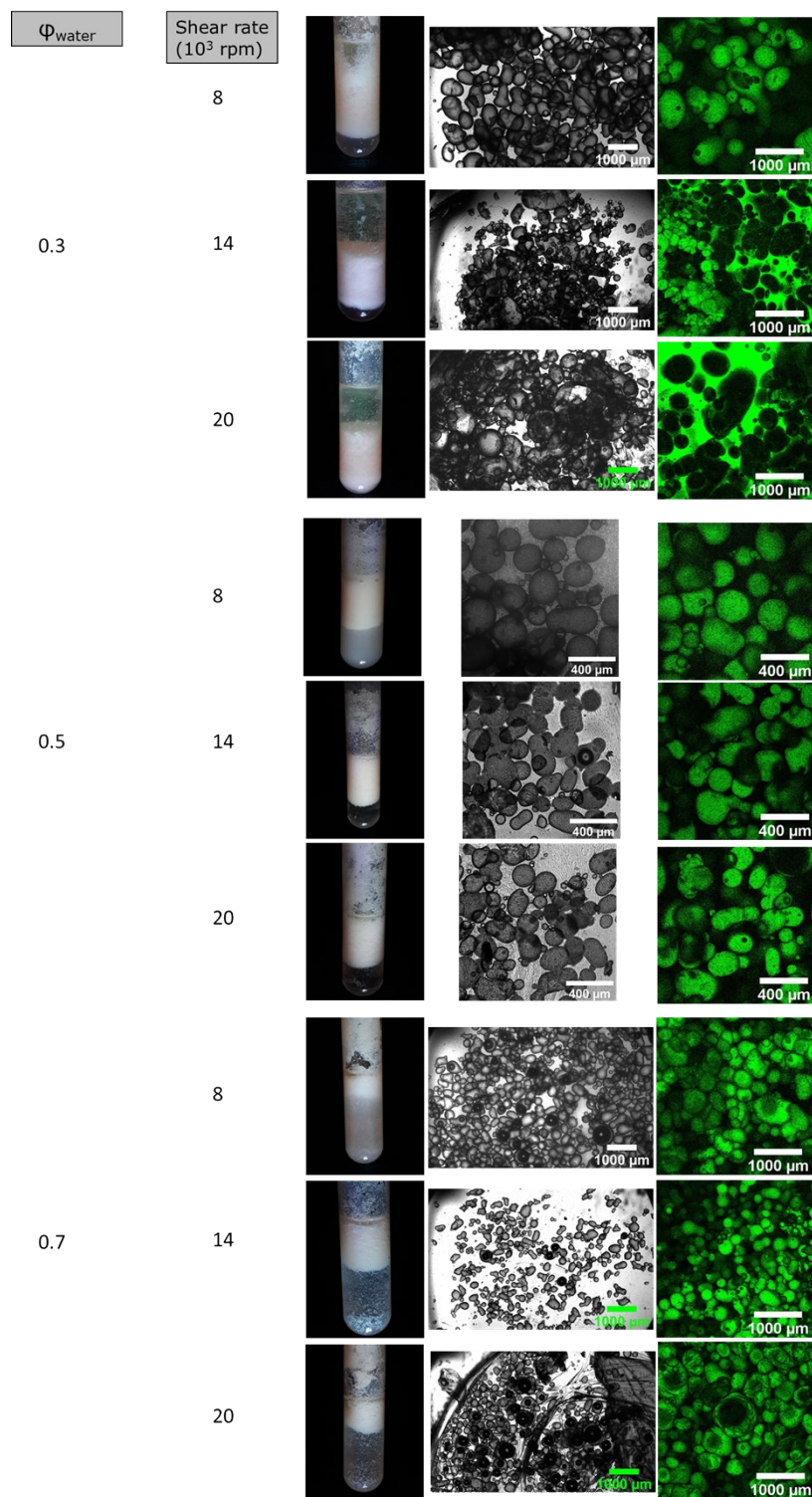


Figure S19. Images of emulsions with RB-7.5. From the left to the right column: macroscopic, bright field optical microscopy and confocal fluorescence microscopy images. The confocal fluorescence microscopy images show whether the emulsions are o/w or w/o type by addition of BODIPY 493/503 to the n-decane oil phase.

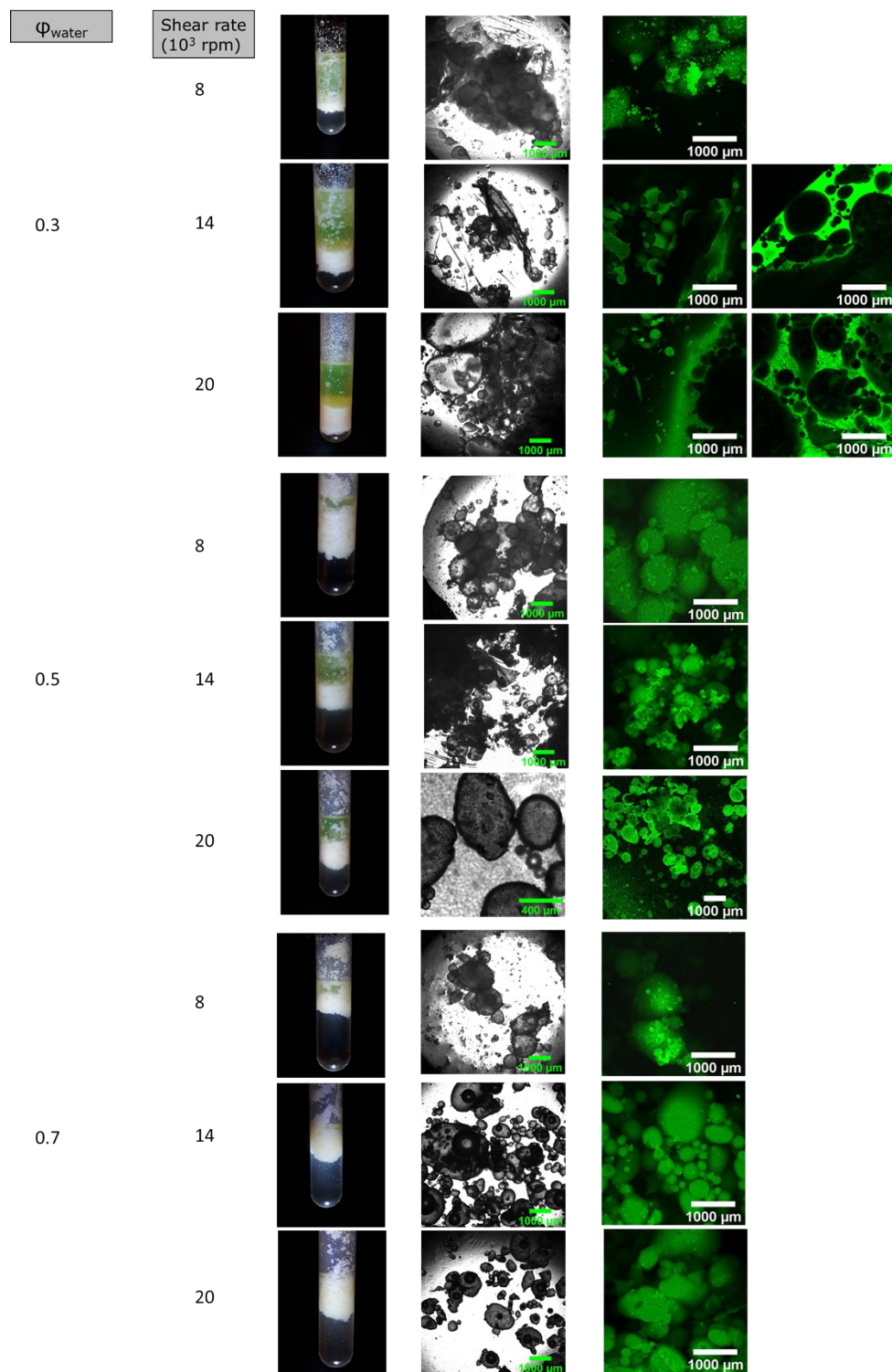


Figure S20. Images of emulsions with RB-16. From the left to the right column: macroscopic, bright field optical microscopy and confocal fluorescence microscopy images. The confocal fluorescence microscopy images show whether the emulsions are o/w or w/o type by addition of BODIPY 493/503 to the n-decane oil phase.

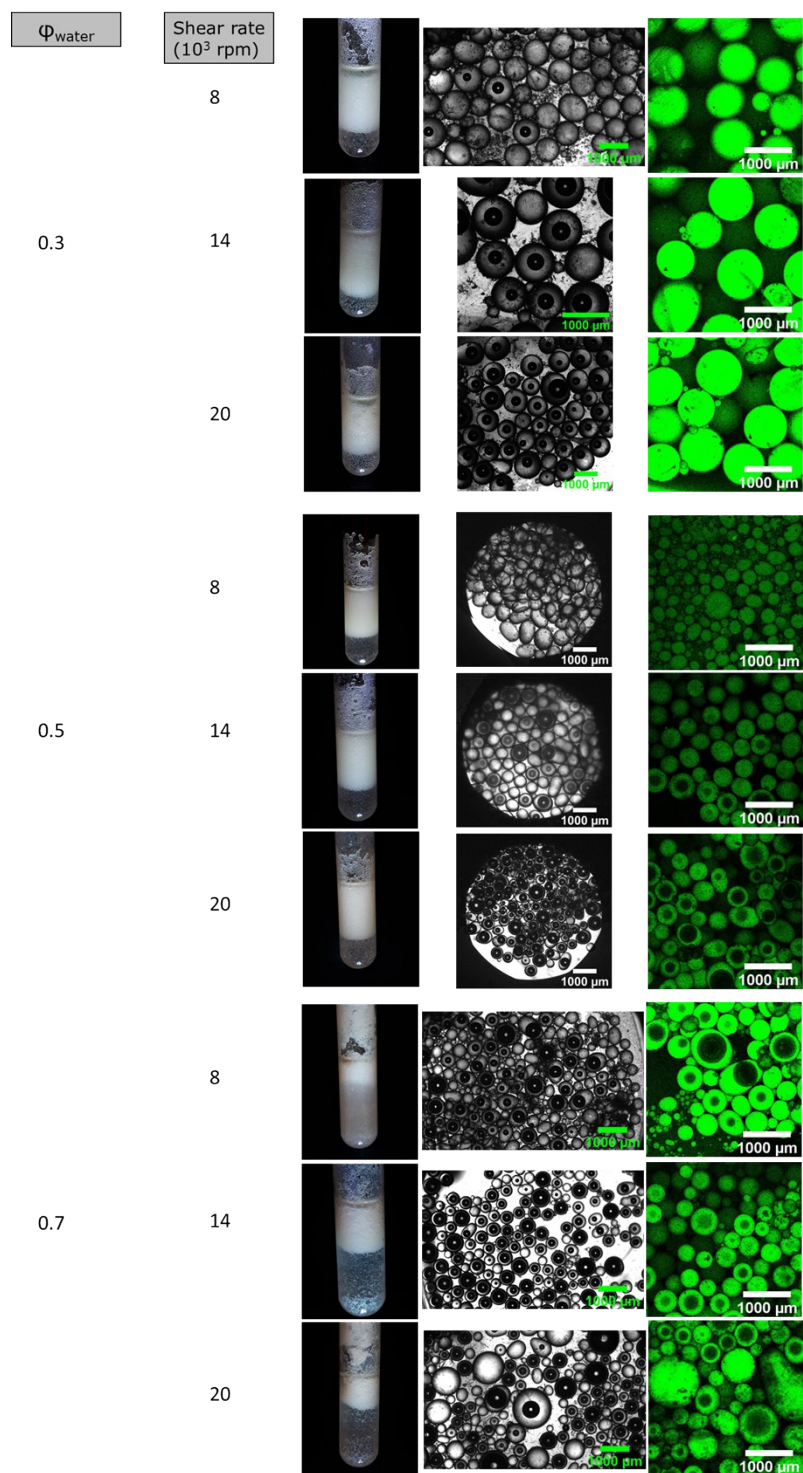


Figure S21. Images of emulsions with TPM. From the left to the right column: macroscopic, bright field optical microscopy and confocal fluorescence microscopy images. The confocal fluorescence microscopy images show whether the emulsions are o/w or w/o type by addition of BODIPY 493/503 to the n-decane oil phase.

REFERENCES

- 1 T. F. Tadros, in *Emulsion Formation and Stability*, ed. T. F. Tadros, WILEY-VCH Verlag GmbH & Co. KGaA, 1st ed., 2013.
- 2 J. D. Berry, M. J. Neeson, R. R. Dagastine, D. Y. C. Chan and R. F. Tabor, *J. Colloid Interface Sci.*, 2015, **454**, 226–237.
- 3 H. Wang, V. Singh and S. H. Behrens, *J. Phys. Chem. Lett.*, 2012, **3**, 46.
- 4 A. San-Miguel and S. H. Behrens, *Langmuir*, 2012, **28**, 12038–12043.